Nuclear Instruments and Methods 174 (1980) 257–269
© North-Holland Publishing Company

A MONTE CARLO COMPUTER PROGRAM FOR THE TRANSPORT OF ENERGETIC IONS IN AMORPHOUS TARGETS *

J.P. BIERSACK
Hahn-Meitner-Institut, Berlin 39, Germany

and

L.G. HAGGMARK †
Sandia Laboratories, Livermore, California, U.S.A.

Received 7 November 1979 and in revised form 18 February 1980

The formalism for a Monte Carlo computer program which simulates slowing down and scattering of energetic ions in amorphous targets is presented. It was developed for determining ion range and damage distributions as well as angular and energy distributions of backscattered and transmitted ions. The computer program provides particularly high computer efficiency, while still maintaining a high degree of accuracy. This is achieved mainly by applying a new analytic formula for determining nuclear scattering angles based on the Molière potential, and by suitably expanding the distance between collisions at high energies. With these improvements it becomes feasible for the first time to assess accurately both low and high energy problems with high precision using a single simulation program.

1. Introduction

The computer simulation of the slowing down and scattering of energetic ions in materials has been used recently in studies of ion implantation, radiation damage, sputtering, and the reflection and transmission of ions. The Monte Carlo method as applied in simulation techniques has a number of distinct advantages over present analytical formulations based on transport theory. It allows more rigorous treatment of elastic scattering, explicit consideration of surfaces and interfaces, and easy determination of energy and angular distributions. The major limitation of this method is that it is inherently a computer-time consuming procedure. Thus there is often a conflict between available computer time and desired statistical precision. In the Monte Carlo computer program presented here, we attempt to alleviate this problem by using techniques which reduce computer usage by at least an order of magnitude and at the same time sacrifice little accuracy.

* This work was supported in part by the U.S. Department of Energy.

† Guest Scientist at the Hahn-Meitner-Institut, Berlin 39, Germany, during the period this work was being completed.

Several ion transport procedures based on the Monte Carlo method have been reported [1–9]. Aside from considering crystalline or amorphous targets, their major differences lie in their treatment of elastic or nuclear scattering. Only Oen, Robinson, and coworkers [3,4] treat this scattering in a precise manner by numerically evaluating the classical scattering integral for realistic interatomic potentials. Other authors [5–9] base their formalisms on either the momentum approximation extended to large angles [5,6] or fitted, truncated Coulomb potentials [7–9] to obtain analytical representations of the scattering integral. Since energetic ions undergo many collisions in the process of slowing down, the method used to evaluate the scattering integral is of critical importance in terms of its relative computer efficiency. Therefore, we have made use of a new analytic scheme which very accurately reproduces scattering integral results for realistic potentials.

As with other simulation programs, our method consists of following a large number of individual ion or particle "histories" in a target. Each history begins with a given energy, position, and direction. The particle is assumed to change direction as a result of binary nuclear collisions and move in straight free-flight-paths between collisions. The energy is reduced

as a result of nuclear and electronic (inelastic) energy losses, and a history is terminated either when the energy drops below a pre-specified value or when the particle's position is outside the target. The target is considered amorphous with atoms at random locations, and thus the directional properties of the crystal lattice are ignored. This method is applicable to a wide range of incident energies–approximately 0.1 keV to several MeV, depending on the masses involved. The lower limit is due to the inclusion of binary collisions only, while the upper limit results from the neglect of relativistic effects. Also, nuclear reactions are not included. The efficiency for dealing with high energy particles has been increased by introducing an energy dependent free-flight-path. Thus, a particle's free-flight-path between collisions is longer at high energies and is steadily reduced in the course of slowing down.

The nuclear and electronic energy losses or stopping powers are assumed to be independent. Thus, particles lose energy in discrete amounts in nuclear collisions and lose energy continuously from electronic interactions. For low energies, where nuclear scattering and energy loss is particularly important, the program utilizes the above mentioned analytic scheme based on the Molière [10] interatomic potential. The unscreened Coulomb potential was found to be sufficient for this scattering at high energies. The low energy, electronic energy loss is based on the velocity dependent treatment of Lindhard and Scharff [11], and at high energies the Bethe-Bloch formulation is used. The interpolation scheme of Biersack [12,13] is used to bridge the gap between the low and high energy regions.

For the sake of computer efficiency, effects of minor influence on range distributions, such as the "time integral" or electronic straggling, which are usually neglected in analytic and Monte Carlo formalisms, have been carefully tested to check whether they can be approximated or neglected. In most cases for energies below 1 MeV, the electronic straggling was found to be of little importance for the projected range profiles. Therefore, in the present program, it is normally neglected, but is available as an option in the form of an impact parameter dependent electronic energy loss. The time integral τ was found to be of little influence in all cases except for the very lowest energies, i.e., below 1 keV. It is therefore included only in an approximate manner with best accuracy at low energies.

The formalism incorporated into the computer programs is applicable to a large variety of ion–target combinations, and the program provides information on ion range and damage characteristics as well as reflection and transmission properties of planar targets. The details of the nuclear and electronic energy loss formulations in the program are presented in section 2 and 3, respectively. Some results of representative calculations are presented in section 4 and compared with experimental data and other calculations. The program has been named TRIM (TRansport of Ions in Matter) and will occasionally be referred to by that name in the text which follows. Another version of this code was developed under the name MORELOVE, and this name is being retained for multilayer targets with multi-atomic compositions [14].

2. Nuclear scattering and energy loss

Nuclear scattering not only is an important process of slowing down the incident particle by momentum transfer to the target atoms, but also determines the spatial distribution of particle trajectories. So far, the only accurate treatment of deflection angles has been a rigorous, numerical evaluation of the classical scattering integral. This method, however, is not feasible for small computers, for high ion energies, or for processing large numbers of histories which may become necessary for certain studies. In these cases, simple analytical expressions of sufficient accuracy are desirable. One such expression of about 1% accuracy has been obtained recently [15]. This expression is used in the present program and will be described here briefly.

2.1. Analytical evaluation of the scattering angle

Fig. 1 depicts the scattering, through an angle θ in the center-of-mass (CM) system, of an incident particle of mass M_1 and kinetic energy E by an initially stationary particle of mass M_2 for a repulsive interaction potential. Superimposed upon the orbits of the two particles is what we call the "scattering triangle". This triangle is comprised of the known or easily accessible quantities P (impact parameter), r_0 (distance of closest approach), ρ_1, ρ_2 (radii of curvature of the trajectories at closest approach), and usually small "correction terms," δ_1 and δ_2. From the scattering triangle it follows immediately that

$$\cos\frac{\theta}{2}=\frac{\rho+P+\delta}{\rho+r_0}\,, \quad \text{with} \begin{cases}\rho=\rho_1+\rho_2\,,\\ \delta=\delta_1+\delta_2\,.\end{cases} \tag{1}$$

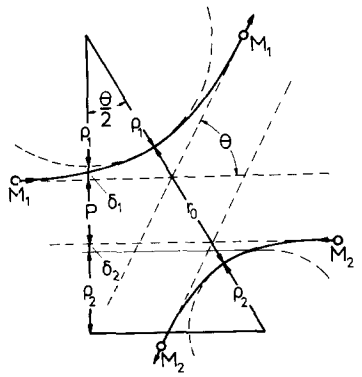

Fig. 1. The particle trajectories in the CM system with superimposed "scattering triangle," comprised of impact parameter P, radii of curvature ρ_1 and ρ_2, distance of closest approach r_0, and the correction terms δ_1 and δ_2. From this construction $\cos(\theta/2)$ is obtained.

The distance of closest approach r_0 is obtained as usual from the relation

$$1 - \frac{V(r_0)}{E_c} - \left(\frac{P}{r_0}\right)^2 = 0 , \tag{2}$$

where $E_c = E/(1 + M_1/M_2)$ is the energy available in the CM system and $V(r)$ the interaction potential between the incident ion and the target atom. Eq. (2) can be solved by Newton's method in 2–4 iterative steps to an accuracy of better than 0.1%. The radius of curvature in the CM system is obtained simply by applying the elementary rule for the centrifugal force f_c. Thus for particle velocities v_1 and v_2 in the CM system, we obtain

$$\rho = \rho_1 + \rho_2 = (M_1 v_1^2 + M_2 v_2^2)/f_c , \tag{3}$$

where the kinetic energy and force may be expressed in terms of E_c and V to yield

$$\rho = \frac{2[E_c - V(r_0)]}{-V'(r_0)} , \tag{4}$$

where $V'(r_0)$ is the spatial derivative of the potential evaluated at r_0.

It is convenient here to express the energy E_c in units of $Z_1 Z_2 e^2/a$ and the length in units of a. Thus we introduce the dimensionless "reduced" energy

$$\epsilon = \frac{a E_c}{Z_1 Z_2 e^2} , \tag{5}$$

where Z_1 and Z_2 are the incident particle and target atomic numbers, respectively, e is the electronic charge, and a is the screening length. We have chosen to use the Firsov [16] screening length given by

$$a = \frac{0.8853 a_0}{(Z_1^{1/2} + Z_2^{1/2})^{2/3}} , \tag{6}$$

where $a_0 = 0.529$ Å is the Bohr radius. Expressing the various lengths in eq. (1) in units of the screening length, we define

$$B = P/a , \quad R_0 = r_0/a , \quad R_c = \rho/a , \quad \text{and } \Delta = \delta/a , \tag{7}$$

so that eq. (1) becomes

$$\cos\frac{\theta}{2} = \frac{B + R_c + \Delta}{R_0 + R_c} . \tag{8}$$

2.2. Fitting formula for Δ

In the high energy limit, atomic collisions can be adequately described using the unscreened Coulomb interatomic potential, i.e., Rutherford scattering. Therefore, a formula for Δ should asymptotically approach the Rutherford result as ϵ becomes large. In achieving this goal we first derived a formula for Δ for Rutherford scattering, and then suitably parameterized this formula for the purposes of fitting it to precomputed scattering results. This procedure leads to the following expression

$$\Delta = A \frac{R_0 - B}{1 + G} , \tag{9}$$

with

$$A = 2\alpha\epsilon B^{\beta} \quad \text{and} \quad G = \gamma[(1 + A^2)^{1/2} - A]^{-1} , \tag{10}$$

where

$$\alpha = 1 + C_1 \epsilon^{-1/2} ,$$

$$\beta = \frac{C_2 + \epsilon^{1/2}}{C_3 + \epsilon^{1/2}} , \tag{11}$$

$$\gamma = \frac{C_4 + \epsilon}{C_5 + \epsilon} ,$$

and C_1–C_5 are the fitting parameters to be determined for the potential of interest. Eq. (9) is not a unique expression for Δ, but is was found in the fitting procedure that this form containing the factor $(R_0 - B)$ gave the best fit and the most stable result. Note as ϵ becomes sufficiently large α, β and γ approach unity and eq. (9) reproduces Rutherford scattering as is desired.

2.3. Interatomic potential

A recent study by Wilson et al. [17] has shown that the Molière approximation [10] to the Thomas–Fermi potential is a more suitable universal potential for nuclear stopping than say the Bohr [18] or Sommerfeld [19] (Thomas–Fermi) potential, particularly for low ϵ values. Therefore we have adopted the Molière potential for nuclear scattering and energy loss at low energies in our ion transport simulation. This potential is given by

$$V(R) = \frac{Z_1 Z_2 e^2}{aR} \cdot \Phi(R), \tag{12}$$

where R is the reduced interatomic separation, $R = r/a$ and $\Phi(R)$ is Molière's screening function:

$$\Phi(R) = 0.35 \exp(-0.3R) + 0.55 \exp(-1.2R) + 0.1 \exp(-6R). \tag{13}$$

Robinson [20] has tabulated the solutions of the classical scattering integral for the Molière potential for a wide range of ϵ and B values. These tables include R_0 and θ as well as $\sin^2(\theta/2)$. Using these tables, we determined the parameters necessary for eqs. (9)–(11) by minimizing in the least-squares sense, the ratio of the fitted to tabulated $\sin^2(\theta/2)$ values. This quantity was selected for use in the fitting procedure because the nuclear energy loss is proportional to $\sin^2(\theta/2)$. The parameters were determined from Robinson's data set at $\epsilon = 10^{-5}$, 10^{-4}, 10^{-3}, 10^{-2}, 10^{-1}, 10^{0} and 10^{1} and B values from 0 to its maximum value at each value of ϵ.

Table 1 gives the values determined for the five parameters indicated in eq. (11) for the Molière potential. Figs. 2a and 2b show $\sin^2(\theta/2)$ as a function of the impact parameter B for the above listed values of ϵ. In the figures, the solid lines have been drawn through Robinson's tabulated results and the circled points represent the values based on the formulation presented here. Also shown in fig. 2b, for comparison purposes are the Rutherford scattering results at $\epsilon = 10$, which will be discussed below. In these semilog graphs it is difficult to perceive the differences between the fitted and tabulated results, but discrepancies as large as ~5% exist. However, discrepancies this large are the exception rather than the rule in the cases examined. The detailed examinations indicate most differences are ~1% or less and the mean deviation is 1.4%. This quality of the agreement between the fitted results and the detailed calcula-

Table 1
Values for constants in eq. (11) based on the Molière potential.

C_1	0.6743
C_2	0.009611
C_3	0.005175
C_4	10.00
C_5	6.314

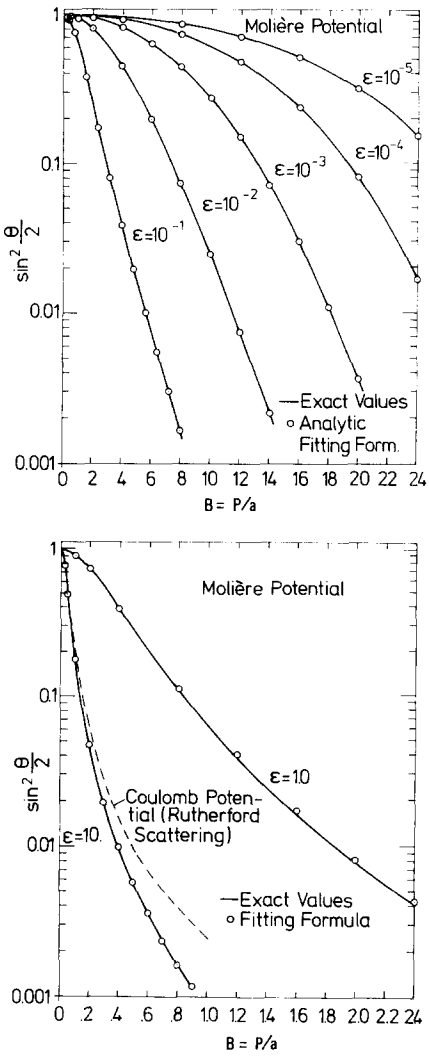

Fig. 2. $\sin^2(\theta/2)$ as a function of impact parameter for reduced energies between 10^{-5} and 10. The circled points have been obtained through our approximate analytical formula derived from the "scattering triangle." The solid lines represent the exact results from ref. 20. The dashed line for $\epsilon = 10$ is drawn for an unscreened Coulomb potential for comparison.

tions over at least 6 orders of magnitude in ϵ is considered quite satisfactory, and since it asymptotically approaches the proper limit for large ϵ, this provides some justification for the detailed, five parameter formulation that has been used to achieve these results.

Even though the above formalism for nuclear scattering based on the Molière potential has built-in validity for large values of ϵ, we have decided, for the sake of the computer efficiency, to base the calculations on the Coulomb potential for $\epsilon > 10$. For the Coulomb potential, $\sin^2(\theta/2)$ is simply related to ϵ and B by the following expression:

$$\sin^2(\theta/2) = [1 + (2\epsilon B)^2]^{-1} . \quad (14)$$

Note in fig. 2b at $\epsilon = 10$ that where $\sin^2(\theta/2)$ is large, i.e., small B, the results for the Coulomb and Molière potentials are quite similar. There exist marked differences only for small values of $\sin^2(\theta/2)$ where the energy loss and angular deflection are small. For example, consider the case near $B = 0.4$ where the ratio of the Coulomb to Molière $\sin^2(\theta/2)$ is 1.5. For equal mass atoms, the incident atom would lose ~1.5% of its energy using the Coulomb potential rather than ~1% with the Molière potential [see eq. (15) below], and its scattering angle in the laboratory system would be ~7° rather than ~6° [see eq. (16) below]. At higher values of ϵ these types of differences become less, and therefore the use of the Coulomb potential for $\epsilon > 10$ should perturb results of calculations only slightly while reducing the computing time.

2.4. Nuclear energy loss and angular transformation

As mentioned previously the nuclear energy loss or energy transfer T to the target atom in a single collision is proportional to $\sin^2(\theta/2)$ and is given by

$$T = 4M_1M_2(M_1 + M_2)^{-2} E \sin^2(\theta/2) . \quad (15)$$

The above formalism for nuclear scattering provides the scattering angle θ in the CM system. The scattering angle ψ in the laboratory system is given by the following relationship:

$$\psi = \arctan\{\sin\theta/[\cos\theta + (M_1/M_2)]\} . \quad (16)$$

The azimuthal scattering angle ϕ is randomly selected using the relation

$$\phi = 2\pi R_n , \quad (17)$$

where R_n is a random number uniformly distributed between 0 and 1.

In actual calculations the particles are followed with reference to a fixed axis, the target normal. The angle α with respect to this axis is determined after each collision. The cosine of this angle, after the ith collision, is given by

$$\cos\alpha_i = \cos\alpha_{i-1}\cos\psi_i + \sin\alpha_{i-1}\sin\psi_i\cos\phi_i . \quad (18)$$

2.5. Distance between collisions and impact parameter selection

At high energies, $\epsilon \gg 10$, only few of the many encounters in the target cause significant deflections from the straight path of flight. Even over distances L large compared to the interatomic distance in a solid, a noticeable deflection ($\psi > 1°$) is a rare event, connected with a very small impact parameter. Therefore, the program is set up to select the smallest impact parameter which occurs over the path length L, and neglect the other collisions with larger impact parameters and smaller deflection angles. The smallest impact parameter over the path length L is found in the following way: The probability $W_1(P)\,\delta P$ for finding a target atom a a radial distance between P and $P + \delta P$ is

$$W_1(P)\,\delta P = NL2\pi P\,\delta P , \quad (19)$$

where N is the atomic density of the target. The probability for not finding another atom closer than P, i.e., between 0 and P, is

$$W_2(P) = e^{-NL\pi P^2} . \quad (20)$$

Hence, the probability for finding the closest target atom between P and $P + \delta P$, i.e., finding an atom there, provided no one is closer, becomes the product

$$W(P)\,\delta P = W_2(P)\,W_1(P)\,\delta P = e^{-NL\pi P^2} NL2\pi P\,\delta P \quad (21)$$

This probability distribution leads to the impact parameter determination

$$P = [-\ln(R_n/\pi NL]^{1/2} \quad (22)$$

from random numbers R_n which are evenly distributed between 0 and 1.

For high energies, the length L is chosen such that the mean angular deflection per path length L remains about constant, i.e.,

$$\frac{M_2}{M_1}\frac{\Delta E_n}{E} = \frac{M_2}{M_1}\frac{LS_n(E)}{E} = \text{constant} , \quad (23)$$

according to the Bohr [18]–Williams [21] rule. Introducing the recently determined analytic expres-

sion for the nuclear stopping power S_n for the Molière potential [17] and choosing the constant in eq. (23) to yield an average deflection of about 5° per path interval L; we obtain from eq. (23)

$$L = \frac{0.02[1 + (M_1/M_2)]^2}{4\pi a^2 N} \frac{\epsilon^2 + 0.052\epsilon^{1.32}}{\ln(1+\epsilon)} . \quad (24)$$

By choosing the free flight path in this way, one is assured that $L(E)$ is always short compared to the mean distance between large angle deflections ($\psi > 10°$). Therefore, it does not matter where such a deflection occurs within each L-interval. Normally, deflection angles are small and account for the "multiple scattering" which gradually changes the direction of the ion's motion. In the high energy region, a second independent check is performed on the path length L in order to ensure that the electronic energy loss does not exceed 5% of the ion energy. In cases where this should happen (e.g., high energy light particles), the path length L is reduced accordingly.

For low energies, where by virtue of eq. (24) the free path L becomes less than $N^{-1/3}$, the approximate mean atomic separation $N^{-1/3}$ is used for L instead. In this case, however, the impact parameter has to be chosen according to

$$W(P)\,\delta P = \begin{cases} 2\pi N^{2/3} P \delta P , & \text{for } P < \pi^{-1/2} N^{-1/3} , \\ 0 , & \text{for } P > \pi^{-1/2} N^{-1/3} , \end{cases} \quad (25)$$

since now only one atom is assumed in the volume element of length $N^{-1/3}$ and base area of $N^{-2/3}$. This procedure maintains the atomic density in the target without correlating the lateral positions of successive target atoms (neglection of lattice structure). This assumption, eq. (25), leads to the determination of impact parameters

$$P = [R_n/(\pi N^{2/3})]^{1/2} . \quad (26)$$

With the impact parameter selections eqs. (22) and (26), a discontinuity in the treatment is created at the transition from the "high energy" to the "low energy" part of slowing down. Being aware of this, we have performed tests on the range distribution of 100 keV B^+ in silicon, and on reflected particles and energies for 2–20 keV He^+ incident on copper. No difference could be found in the results when using the prescribed procedure or when using a fixed value for the free flight path ($L = N^{-1/3}$) throughout the slowing down process.

Also, another check was performed on using a realistic distribution of L values, e.g. between $a/\sqrt{2}$ and $a/2$ in an f.c.c. lattice, rather than the fixed value $L = N^{-1/3}$ ($=a/2^{2/3}$ for f.c.c. lattices). However, no difference in the results could be detected, and the fixed value was chosen for best efficiency.

At very low energies, e.g., less than 200 eV for He^+ incident on Cu, the free flight path of the ion becomes less than the distance to the next target atom, since the deflection point of the ion trajectory lies *in front* of the target's center. This can best be visualized by assuming hard sphere collisions. Indeed, comparative tests showed that the hard sphere approximation yields a sufficient accurate estimate for this effect. Therefore, at low energies, $L = N^{-1/3} - P \tan(\theta/2)$ is used to account for the path-length reduction. (In the literature this offset is referred to as the "time integral τ" and is given by an integral expression similar to the scattering integral.)

3. Electronic energy loss

In the high energy region, the inelastic or electronic energy loss is treated independent of the nuclear energy loss, as in all previous ion transport theories and models. The reasons for neglecting the correlation between the elastic and inelastic energy losses in our case are twofold. The pragmatic reason is the increased computer efficiency, mainly through the applicability of our concept of extended free flight paths. The other, more important reason is the lack of satisfactory theoretical descriptions or experimental data of the impact parameter dependence of the electronic energy loss.

Neglecting impact parameter dependence and straggling at high energies, we simply relate the electronic energy loss to the distance L travelled between collision by

$$\Delta E_e = L N S_e(E) , \quad (27)$$

where $S_e(E)$ is the electronic stopping cross section which equals at low energies

$$S_L = kE^p , \quad (28)$$

where k is the velocity independent stopping parameter. We use mainly the Lindhard–Scharff [11] formula

$$k = k_L = \frac{1.212 Z_1^{7/6} Z_2}{(Z_1^{2/3} + Z_2^{2/3})^{3/2} M_1^{1/2}} \ \mathrm{eV^{1/2}\,\AA^2} , \quad (29)$$

$$p = 1/2 ,$$

which approximates very well the general trends in

the Z_1 and Z_2 dependencies. Deviations are known to exist (Z_1 or Z_2 "oscillations" [22]) and–if known for the paricular case–can be taken into account by an appropriate correction factor k/k_L and choice of p.

For ion velocities $v > v_0 Z_1^{2/3}$ and $v > v_0 Z_2^{1/2}$, $v_0 = e^2/h = c/137$, the Bethe–Bloch electronic stopping formulation becomes valid. For nonrelativistic energies this stopping cross section can be expressed as

$$S = \frac{8\pi Z_1^2 e^4}{I_0 \epsilon_B} \ln \epsilon_B , \quad \text{with } \epsilon_B = \frac{2m_e v^2}{Z_2 I_0} , \tag{30}$$

where m_e is the electron mass and $Z_2 I_0$ is the mean excitation energy. The Bloch constant I_0 can be represented [23] by

$$I_0 = \begin{cases} 12 + 7Z_2^{-1} , \\ 9.76 + 58.5 Z_2^{-1.19} , \end{cases} \quad \text{for } Z_2 \begin{cases} < 13 , \\ \geqslant 13 . \end{cases} \tag{31}$$

While following the ion from high to low energies, one has to deal with the transition region between the domains of validity of the above eqs. (28) and (30). In order to bridge the gap between the high and low energy regions and to provide a realistically smooth transition, we apply the interpolation scheme as proposed by Biersack [12,13]

$$S_e = (S_L^{-1} + S_B^{-1})^{-1} , \tag{32}$$

with S_L given in eq. (28) and S_B slightly modified from eq. (30) in order to obtain an overall sufficient fit with experimental data in the transition region:

$$S_B = \frac{8\pi Z_1^2 e^4}{I_0 \epsilon_B} \ln(\epsilon_B + 1 + C/\epsilon_B), \quad C = 5 . \tag{33}$$

For $Z_1 < 3$, $C = 100 Z_1/Z_2$ is used in the program which yields a better fit to experimental data. The value of C is not very critical, as it comes into play only at low energies, where it is already masked by the Lindhard–Scharff stopping power S_L.

At low energies, one might consider the use of an electronic loss which is correlated with the impact parameter of each collision. Expressions for the electronic energy loss as a function of impact parameter P or of the distance of closest approach r_0 have been provided by Firsov [24] and by Oen and Robinson [25]. Firsov's derivation assumes about equal size of ion and target atom, and is therefore restricted in validity to

$$1/4 < Z_1/Z_2 < 4 ,$$

$$\Delta E_e = \frac{4.3 \times 10^{-8} (Z_1 + Z_2)^{5/3} v}{[1 + 0.31 P (Z_1 + Z_2)^{1/3}]^5} \tag{34}$$

where v(cm/s) is the ion velocity and P(Å) the impact parameter.

Oen and Robinson have suggested

$$\Delta E_e = \frac{0.045 k\sqrt{E}}{\pi a^2} e^{-0.3 r_0/a} , \tag{35}$$

where $k\sqrt{E}$ is the electronic stopping cross section in the low energy regime, and the forefactor is chosen such that at higher energies, when $r_0 \to P$, the full electronic stopping is retrieved.

Eq. (35) has been made available as an option in the TRIM program. We prefer Oen's and Robinson's formalism for the following reasons: (1) it has no restrictions in the Z_1/Z_2 ratio, (2) it accounts for the real ion trajectory by considering a closest approach of r_0 rather than P, and (3) it was found to yield about the right amount of total electronic straggling, as compared to current theoretical predictions. Applying this option to low energy light ions, most drastic changes are seen in the path-length distribution, e.g. for 8 keV protons in a gold target, the total path length is increased nearly 50%, and the path length straggling is increased about 5 times. However, the physically observable distributions, e.g. projected ranges or backscattered particles, undergo only minor (<15%) changes. For heavy ions these effects become completely negligible, as the slowing down becomes dominated by nuclear stopping.

4. Results and comparisons

To demonstrate the applicability and reliability of the transport model which has been outlined in the previous sections, a number of representative calculations have been performed with the computer program. We have tried to select cases which have some intrinsic interest, and, in addition, have been studied previously, either experimentally or by other computational methods. With this in mind results are presented for the following ion–target combinations: B–Si, Sb–Si, ^{3}He–Nb, and ^{4}He–Cu. In all cases the ions are normally incident on the targets. A minimum of 1000 particle histories were followed, and in some instances, as many as 5000 histories were processed, particularly where the details of the depth distribution were of interest. Generally, a history was terminated when the ion energy decreased below 10 eV, but for some low ion energies, this cutoff energy was lowered to 5 eV.

4.1. Boron–silicon

The B–Si ion–target combination is particularly noteworthy as a test for a computational technique since it has been investigated previously on a number of occasions. Several measurements of the projected range distributions have been reported using different experimental techniques. Brice [26] and Gibbons et al. [27] have tabulated their theoretical predictions of the projected range and range statistics for this ion–target combination based on the moments method. They both used the measured electronic stopping power of Eisen [28] to correct the Lindhard–Scharff [11] stopping power formula, i.e., $k/k_L = 1.59$. We have used this same correction to the electronic stopping power and performed calculations for this system for energies from 30 to 200 keV. Fig. 3 shows the TRIM results for the projected range R_p (mean range) and the standard deviation σ of the range distribution as a function of ion energy. Also shown in this figure are the experimental results of Hofker et al. [29] and Ryssel et al. [30] and the theoretical results of Brice [26]. A smooth curve has been drawn through Brice's results, and the TRIM and experimental results are represented by the indicated symbols. The theoretical results of Gibbons et al. are not included since they are essentially identical to those of Brice. We feel there is reasonable agreement between our results and those of the experiments and the other calculations.

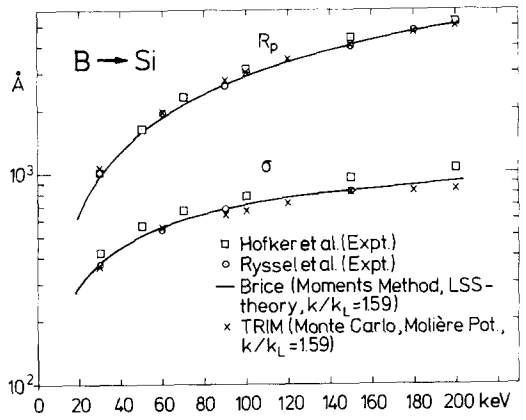

Fig. 3. Mean projected range R_p and standard deviation σ for 20–200 keV boron implanted into silicon. Crosses indicate present results (Monte Carlo code TRIM) which are compared (1) with recent experimental results (circles obtained from (n, α)-depth profiling [30], squares from SIMS measurements [29]) and (2) with analytic moment calculations [26] (full lines). All theoretical values use 1.59 times the Lindhard–Scharff electronic stopping [28].

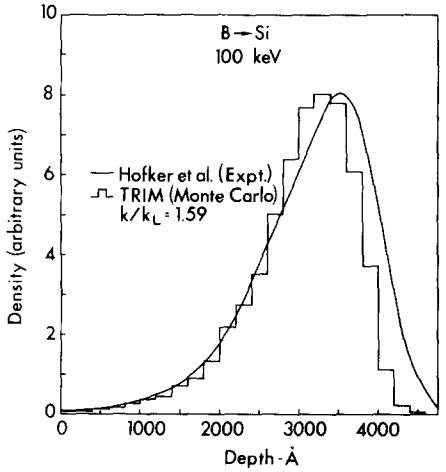

Fig. 4. 100 keV boron depth distributions in silicon: Histograms represent Monte Carlo results (TRIM), and the full line represents the experimental data [29]. The agreement of the shapes of the distributions is evident, whilst the absolute values for mean projected range and standard deviation could be improved by choosing a smaller electronic stopping than prescribed by Eisen [28].

Our results for the projected range distributions for 100 keV boron ions incident on silicon is shown in fig. 4 along with the experimental distributions of Hofker et al. Both of these distributions are slightly skewed to the right, but the mode and width of TRIM results are slightly smaller than those of the experiment. Hofker et al. have indicated that their measurements are more consistent with $k/k_L = 1.5$ for the electronic stopping. Indeed, we also get better agreement with their experiment using this value.

4.2. Antimony–silicon

Oetzmann et al. [31] have recently extended their precise range measurements down to low values of ϵ by implanting heavy ions in silicon and germanium. For these cases, the nuclear stopping dominates the slowing down process, and thus they provide a stringent test for any theory of nuclear scattering and energy loss. Calculations were performed for Sb ions incident on Si targets for energies from 5 to 100 keV. The projected range results from these calculations are shown as a function of energy in fig. 5 together with the experimental results of Oetzmann et al. and the theoretical results of Brice [26]. The TRIM results range from 10 to 20% lower than those of the experiment. This indicates that even the Molière

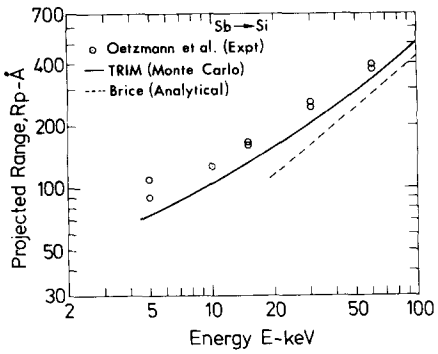

Fig. 5. Projected ranges of antimony in silicon. Circled points represent experimental data of Oetzmann et al. [31], solid curve was drawn through present TRIM results, and dashed line depicts results from analytic theory [26]. In this case of heavy ions, the electronic stopping is of very little importance and the discrepancy between theory and experiment clearly indicates that a weaker than Molière potential is necessary.

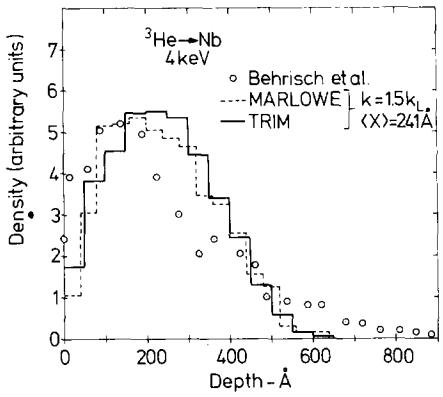

Fig. 6. Range distribution of 4 keV He ions in niobium. At this low energy, the leakage of particles through the surface in the slowing-down process results in the sharp drop towards the surface which is clearly visible in the Monte Carlo histograms (present calculation: full line, MARLOWE [34]: dashed Experimental points from Behrisch et al. [33].

potential is not completely adequate for the formulation of nuclear stopping in these cases, but use of this potential provides better results than the Lindhard et al. [32] nuclear stopping theory which is used in Brice's calculations. These conclusions are consistent with the recent theoretical study of Wilson et al. [17] who investigated the effects of the interatomic potential on the nuclear stopping power.

4.3. ^{3}Helium–niobium

The recent investigations of the radiation damage problems associated with first walls of future fusion reactors has generated interest in light ions incident on metals. Niobium is one of the metals that has been studied extensively in this regard. We present here the results of two calculations of the projected range distributions–at 4 and 150 keV–for ^{3}He ions incident on Nb targets. The 4 keV case is shown in fig. 6 together with the experimental results of Behrisch et al. [33] and the Monte Carlo calculation of Oen and Robinson [34] (MARLOWE [4] program). Both the TRIM and MARLOWE results are based on k/k_L = 1.5 for electronic stopping. There is substantial agreement between the two calculations but neither is able to reproduce the experimental data. This seems to provide some justification for further experimental measurements to resolve the discrepancies, although it is realized that these measurements for low energy implanted ions are difficult.

The projected range distribution for the 150 keV case is shown in fig. 7 along with the recent measurement of Biersack et al. [35]. Again, $k/k_L = 1.5$ is used for our calculation. The shapes and mean values of these two distributions are quite similar although the calculated distribution is noticeably narrower. It should be noted that the detector resolution has not been removed from the experimental distribution. If

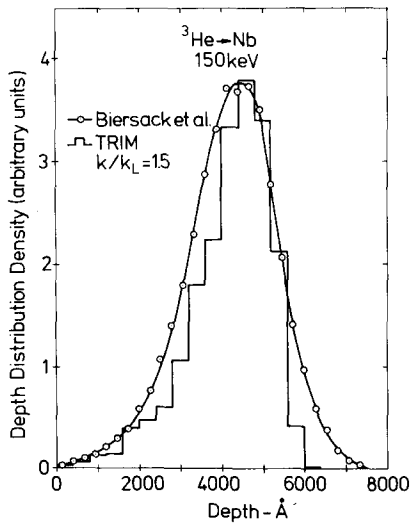

Fig. 7. Range distribution of 150 keV ^{3}He in niobium. Experimental data [35] (line through circled points) in comparison with present Monte Carlo results (histogram). Agreement is satisfactory, but could still be improved by deconvoluting experimental data with the detector resolution function.

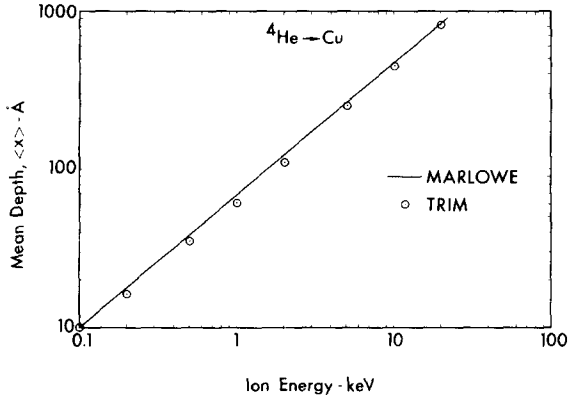

Fig. 8. Mean projected ranges of low energy helium ions impinging on copper. Comparisons of present Monte Carlo results (circled points) with those of Oen and Robinson [25] (full line) show agreement within statistical errors for all energies.

this deconvolution were carried out, there would be substantial improvement in the agreement between the two results.

4.4. *Helium–copper*

Oen and Robinson [25,34] have recently produced a large amount of data for low energy, light ions incident on amorphous metal targets using the MARLOWE [4] Monte Carlo program (one example of this was presented above). To provide further direct comparisons with this more sophisticated simulation procedure, we have performed calculations for ^{4}He ions incident on Cu targets for ion energies from

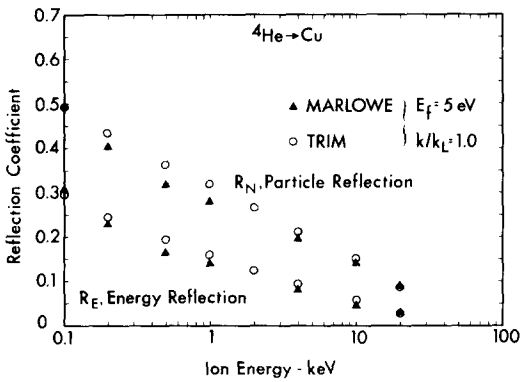

Fig. 9. Particle reflection and energy reflection for low energy He on copper. A comparison of present results with those of Oen and Robinson [25] indicate that both particle and energy reflection coefficients (backscattered fractions) are identical within statistical errors.

0.1 to 20 keV. Fig. 8 shows the mean penetration depth $\langle X \rangle$ as a function of ion energy. A solid line has been drawn through the MARLOWE [34] results and the circled points represent the TRIM results. The two results agree with ~10%, however the TRIM results are systematically lower which is attributed to the different treatment of the electronic energy loss. The ^{4}He–Cu backscatter coefficients as a function of the incident ion energy are shown in fig. 9. For the particle and energy reflection coefficients, R_N and R_E, again there is satisfactory agreement, within statistical errors, between the MARLOWE [25] and TRIM results over the energy range considered.

5. Discussion and conclusion

In this paper we have presented the details of a Monte Carlo transport formalism, which is applicable to a wide range of problems involving the slowing down of energetic ions in amorphous materials. There are several features of this program which distinguish it from other binary collision simulation formalisms. One of these is the use of an analytic representation of the low energy nuclear scattering based on a more realistic potential. This allows for a rapid and accurate assessment of an ion's direction and energy loss resulting from nuclear collisions. The other unique feature in the program is the facility at high energies to lengthen the free flight distances between collisions. This allows for the consideration of some higher energy problems with the expenditure of a reasonable amount of computer time. The results of the calculations for a variety of ion–target combinations indicate generally good agreement with experimental measurements and other theoretical results at both high and low energies.

It is our pleasure to acknowledge the skillful help of Mrs. S. Franke in preparing the computer program. The authors are indebted to M.I. Baskes of Sandia Laboratories for his suggestive and able assistance in the development of the fitting formulas used for the nuclear scattering in this work. We are grateful for very valuable discussions with A. Riccato from Technische Universität Berlin and M.T. Robinson from the Oak Ridge National Laboratory. L.G.H. wishes to gratefully acknowledge the hospitality of the Hahn-Meitner Institut für Kernforschung Berlin, Germany, during the period when this work was being completed.

Appendix

In this appendix some practical information on the use of the computer program TRIM shall be provided. The program is written in the language FORTRAN IV and uses only one computer system dependent library function. This function is the random number generator which appears in three statements in the program and which provides random numbers uniformly distributed between 0 and 1.

In the program the unit of energy is the electronvolt (eV) and the unit of length is the ångstrøm (Å). There are 16 input parameters which are read from two computer cards:

Card 1: Z1, M1, Z2, M2, RHO, TT, ED, CK (Format 8F10.2):

Z1 = incident ion atomic number,
M1 = incident ion atomic weight,
Z2 = target atomic number,
M2 = target atomic weight,
RHO = target density (g/cm^3),
TT = target thickness (Å),
ED = energy for displacement of a target atom (eV),
CK = k/k_L correction factor for the low energy electronic stopping power.

Card 2: EO, EF, XO, ALPHA, LO, CW, RI, HN (Format 8F10.0):

EO = incident ion energy (eV),
EF = ion final or cut-off energy (eV),
XO = ion initial position (Å),
ALPHA = ion initial angle with respect to the target normal (degrees),
LO = ion initial mean free flight path between collisions (Å),
CW = channel width of the output depth distributions (Å),
RI = initializer for the random number generator,
HN = number of ion histories to be processed.

Most of these input variables are self evident. The displacement energy ED is the energy necessary for creating a Frenkel pair (a typical value for many metals would be 25 eV). The correction factor for electronic stopping CK is a means to correct for known deviations from the Lindhard–Scharff stopping power (typical values are between 1 and 2). For the final energy EF usually values of 5 or 10 eV are chosen dependent on the initial energy EO and the channel width CW. Starting point and direction XO and ALPHA are used with non-zero values in cases of non-normal ion incidence, simulation of nuclear recoils created in the material or, for example, in order to obtain the transverse profile of the particle distribution with the present one-dimensional code (e.g. XO = 50 × CW and ALPHA = 90°). LO is used as the mean free flight path for the first collisions only if the following checks are positive: first, in the program a check is performed that LO may not exceed the L-value given in eq. (24), a second test is carried out to ensure that the electronic loss per free flight path does not exceed 5% of the ion energy, and finally the program checks that the mean free flight path may not be less than the mean distance between the target atoms. If any of these conditions is violated, the code will atomiatically reset LO to the nearest allowable value. Most users who want fastest computation use for the input of LO any arbitrary high number and let the code readjust this number to the maximum acceptable free flight path. Other users who are interested in low energies often wish to keep the distance between collisions always equal to the atomic spacing in the target and assure this by setting LO = 1 Å, a value which will be increased by the code to the value of LM. The random number initialyzer RI is used to determine whether one wants to repeat the same sequence of random numbers or not in subsequent runs of the same case (it may be unavailable in certain computer systems). The number of histories should be chosen of the order of 1000 for obtaining statistically satisfying results. The number of histories will always be limited by the available computer time. CPU times have been reported to be between one hundredth and one second per ion history dependent only on the available computer system and not so much on the chosen energy.

The output from the program first lists the values of the input variables (with the possible exception of LO which may have been corrected by the program). The next two lines of output give some information relevant to the choice of the free light path, such as the multiple scattering per free flight path and the maximum electronic loss per free flight path. Then some important constants are printed out: LM–the mean distance between target atoms, EPSILON–the initial energy in reduced dimensionless units, A–the Thomas–Fermi–Firsov screening length, K–for the low energy stopping power and IO–the mean ionization energy used in the Bethe formula. The first Monte Carlo result printed in the output is the number and the energy of backscattered particles and the number and energy of transmitted particles. Next, the

global information is given for ions which are stopped in the target material: the projected range distribution is given through its first four moments (average depth, standard deviation, skewness gamma, kurtosis beta), followed by the two first moments of the total path length distribution (average path length and standard deviation), and finally the average number of collisions necessary for slowing down from the initial to the final energy. These averages are only for particles which stop in the target and they will be zero, if all the particles are backscattered and/or transmitted. After this, the individual depth distributions are listed in 100 bins given by the input channel width: The first column gives the depth intervals, the next five columns list the projected range (depths), total path lengths, the electronic energy loss, the nuclear energy losses below ED and finally the energy losses above ED (responsible for the damage), all as a function of depth. The electronic and nuclear energy loss distributions are so far the energy losses of the incident particles only. However, the energy of recoil motion with energies above ED (column 5) is further analysed in the next two columns, indicating the fraction of energy going into ionization caused by the recoiling atoms and in the displacement of atoms (Frenkel pairs). In the standard TRIM version which is described here, the recoils are not individually followed in the Monte Carlo program but their energy contributions to ionization and defect production are determined by standard theory [36] in the analytical approximation of Robinson [37]. From this theory the defect producing energy E_ν is obtained from the transferred energy T of the recoil by

$$E_\nu = \frac{T}{1 + k_d g(\epsilon_d)} , \tag{36}$$

where

$$k_d = 0.1334 Z_2^{2/3} M_2^{-1/2} , \tag{37}$$

$$g(\epsilon_d) = \epsilon_d + 0.40244 \epsilon_d^{3/4} + 3.4008 \epsilon_d^{1/6} , \tag{38}$$

and

$$\epsilon_d = 0.01024 Z_2^{-7/3} T. \tag{39}$$

From the energy E_ν the number of displacements is calculated by the well known "modified Kinchin–Pease" model [38,39]

$$\left.\begin{aligned} \nu &= 1 , && \text{if } E_D \leqslant E_\nu < 2.5 E_D , \\ \nu &= \frac{0.8 E_\nu}{2 E_D} , && \text{if } E_\nu \geqslant 2.5 E_D . \end{aligned}\right\} \tag{40}$$

If the incident ions leave through the rear surface of the target, they are registered as transmitted particles, in this case also a matrix will be printed, giving the angular and energy distribution of such particles. An output of this kind for the backscattered particles is available as an option.

The basic TRIM program described here was kept as short as possible while still providing some useful output information. Of course the program can and has been extended to include two or three space dimensions, to follow the recoil motion for production of damage or for sputtering processes, and there exist versions for layered targets and multi-atomic compositions.

References

[1] M. Yoshida, J. Phys. Soc. Japan 16 (1961) 44.
[2] J.R. Beeler, Jr., and D.G. Besco, J. Appl. Phys. 34 (1963) 2873.
[3] O.S. Oen, D.K. Holmes and M.T. Robinson, J. Appl. Phys. 34 (1963) 302;
M.T. Robinson and O.S. Oen, Phys. Rev. 132 (1963) 2385;
O.S. Oen and M.T. Robinson, J. Appl. Phys. 35 (1964) 2515.
[4] M.T. Robinson and I.M. Torrens, Phys. Rev. B9 (1974) 5008.
[5] T. Ishitani, R. Shimizu and K. Murata, Jap. J. Appl. Phys. 11 (1972) 125 and Phys. Stat. Sol. (b) 50 (1972) 681.
[6] J.E. Robinson, Rad. Eff. 23 (1974) 29.
[7] K. Guttner, Z. Naturforsch. 26a (1971) 1290; K. Guttner, H. Ewald and H. Schmidt, Rad. Eff. 13 (1972) 111.
[8] D.K. Hutchence and S. Hontzeas, Nucl. Instr. and Meth. 116 (1974) 217.
[9] D.A. Eastham, Nucl. Instr. and Meth. 125 (1975) 277.
[10] G. Molière, Z. Naturforsch. A2 (1947) 133.
[11] J. Lindhard and M. Scharff, Phys. Rev. 124 (1961) 128.
[12] J.P. Biersack and D. Fink, in Ion implantation in semiconductors (ed. S. Namba; Plenum Press, N.Y., 1974) p. 211.
[13] J.P. Biersack and D. Fink, in Atomic collisions in solids, Vol. 2 (Plenum Press, N.Y., 1975) p. 737.
[14] J.P. Biersack and S. Franke, to be published.
[15] J.P. Biersack, L.G. Haggmark and M.I. Baskes, to be published.
[16] O.B. Firsov, Zh. EKsp. Teor. Fiz. 33 (1957) 696 [Sov. Phys.-JETP 6 (1958) 534].
[17] W.D. Wilson, L.G. Haggmark and J.P. Biersack, Phys. Rev. B15 (1977) 2458.
[18] N. Bohr, Kgl. Danske Videnskab. Selskab. Mat.-Fys. Medd. 18, no. 8 (1948).
[19] A. Sommerfeld, Z. Physik 78 (1932) 283.
[20] M.T. Robinson, publication of the Oak Ridge National Laboratory, Oak Ridge, Tennessee, USA, Report ORNL-4556 (1970) (unpublished).

[21] E.J. Williams, Proc. Roy. Soc. (London) 169 (1939); Phys. Rev. 58 (1940) 292.
[22] For example, see J.C. Eckardt, W. Meckback and R.A. Baragiola, Rad. Eff. 27 (1976) 179 and references therein.
[23] W.H. Barkas and M.J. Berger, Studies in penetration of charged particles in matter, NAS-NRC Publication 1133, Nuclear Science Series Report 39 (1964) p. 103; R.M. Sternheimer, Phys. Rev. 145 (1966) 247.
[24] O.B. Firsov, Zh. Eksp. Teor. Fiz. 36 (1959) 1517 [Sov. Phys.-JETP 36 (1959) 1076].
[25] O.S. Oen and M.T. Robinson, Nucl. Instr. and Meth. 132 (1976) 647.
[26] D.K. Brice, Ion implantation range and energy deposition distributions (IFI/Plenum, N.Y., 1975).
[27] J.F. Gibbons, W.S. Johnson and S.W. Mylroie, Projected range statistics (Dowden, Hutchinson and Ross, Inc., Stroundsburg, Pa., 1975).
[28] F.H. Eisen, B. Welch, J. Westmoreland, and J.W. Mayer, in atomic collision processes in solids (eds. D.W. Palmer, M.W. Thompson and P.D. Townsend; Pergamon Press, London, 1970) p. 111.
[29] W.K. Hofker, D.P. Oosthoek, N.J. Koeman and H.A.M. DeGrefte, Rad. Eff. 24 (1975) 223.
[30] H. Ryssel, H. Kranz, K. Muller, R.A. Henkelmann and J. Biersack, Appl. Phys. Lett. 30 (1977) 399.
[31] H. Oetzmann, A. Feuerstein, H. Grahmann and S. Kalbitzer, Phys. Lett. 55A (1975) 170.
[32] J. Lindhard, V. Nielsen and M. Scharff, Kgl. Danske Videnskab. Selskab. Mat.-Fys. Medd. 36, no. 10 (1968).
[33] R. Behrisch, J. Bottiger, W. Eckstein, U. Littmark, J. Roth and B.M.U. Scherzer, Appl. Phys. Lett. 27 (1975) 199.
[34] O.S. Oen and M.T. Robinson, in Application of ion beams to materials (Institute of Physics, London, 1976) Conf. Ser. No. 28, p. 329.
[35] J.P. Biersack, D. Fink, P. Mertens, R.A. Henkelmann and K. Muller, Proc. Int. Symp. on Plasma wall interaction, Jülich (Pergamon Press, Frankfurt, 1977) p. 421.
[36] J. Lindhard, V. Nielsen, M. Scharff and P.V. Thomsen, Danske Videnskab. Selskab. Mat.-Fys. Medd. 33, no. 10 (1963).
[37] M.T. Robinson, Nuclear fission reactors (British Nuclear Energy Society London, 1970) p. 364.
[38] P. Sigmund, Rad. Eff. 1 (1969) 15.
[39] M.J. Norgett, M.T. Robinson and I.M. Torrens, Nucl. Eng. Design 33 (1974) 50.